Fatigue Strength of 316 L Stainless Steel Manufactured by Selective Laser Melting

Sepehr Hatami, Taoran Ma, Taina Vuoristo, Jens Bertilsson, and Ola Lyckfeldt

In this study, the fatigue strength of 316 L stainless steel manufactured by selective laser melting (SLM) is evaluated. The effect of powder layer thickness and postmachining is investigated. Specimens were produced with 30 and 50 μm layer thickness and tested under high cycle fatigue in as-printed and postmachined conditions. Examination of the specimens reveals that in the as-printed condition, fatigue strength suffers from high roughness and surface tensile residual stresses as well as defects such as pores and lack of fusion voids. After machining, the fatigue strength was improved due to lower surface roughness, presence of compressive residual stresses, and removal of surface porosity. The results show that increasing the layer thickness (within the range tested) has a minor negative impact on fatigue strength; however, it has a major positive impact on the productivity of the SLM process. In addition, it is clear that the impact of postmachining on fatigue is far greater than that of the layer thickness.

1. Introduction

In recent years, research and development in selective laser melting (SLM) has motivated widespread industrialization of this technology for low production series of small- and medium-size structural components with complex design. One encouraging factor is the static mechanical properties of SLM-fabricated components. With this technology, various materials can be processed to produce near full density parts with static mechanical properties which in certain cases can be higher than their wrought counterparts. For example, the yield and ultimate tensile strength of SLM produced parts made of 316 L stainless steel are higher than those reported for wrought 316 L material (Ref 1, 2). Another motivating factor for adoption of SLM is related to the economic gains associated with the production of parts with an appreciable level of complexity. By considering design guidelines for SLM and with a thorough knowledge of the process, complex components can often be manufactured more economically with SLM than with conventional methods (Ref 3). Furthermore, continuous development and launch of machines with higher production capabilities and precision have facilitated the industrialization of SLM technology for serial production.

In view of the above remarks, it would be reasonable to expect the manufacturing industry to eagerly adopt SLM and replace some of the conventional manufacturing methods. However, to date, the process is mainly used for prototyping, and the rate of industrialization of this technology is much lower than anticipated.

One underlying reason for the slow adoption of SLM is insufficient knowledge of the influence of SLM process variables on the fatigue strength of the final component (Ref 4). This has led to a lack of confidence in the technology among product designers. A thorough knowledge of the fatigue strength of components produced by SLM is vital, considering that at least 90 percent of all service failures due to mechanical cause is related to fatigue (Ref 5).

Variables such as build orientation, layer thickness, powder properties, SLM process parameters, and the type of machine can affect fatigue strength. The fatigue strength of as-printed 316 L stainless steel material is reported to be inferior to its wrought counterpart (Ref 1, 6). However, postoperations such as machining or vibratory treatments improve the fatigue strength of SLM-fabricated specimens (Ref 1, 7). With respect to build orientation, research by Mower and Long shows that at lifetimes of 10^5–10^6 cycles, the fatigue strength of vertically built 316 L specimens is only 30% of the strength of specimens fabricated horizontally (Ref 6). Rakish et al. showed that the fatigue life of horizontally built and postmachined 316 L stainless steel specimens was higher than those built vertically and diagonally (Ref 2). Similarly, Blinn et al. reported higher fatigue strength and lower scatter for horizontally manufactured and postmachined 316 L material as compared to their vertical counterparts (Ref 8). The anisotropic fatigue behavior is speculated to be related to the orientation of defects (Ref 2), layers (Ref 6, 8), and grain structure (Ref 8) with respect to the loading direction. The study by Zhang et al. shows that variation of process parameters such as laser power and scan speed affects the fatigue strength of the material and determines the type and number of defects such as porosity and lack of fusion voids (Ref 9). Lack of fusion voids and unmelted or partially melted powder particles seem to be common fatigue initiation sites in 316 L stainless steel produced by SLM (Ref 2). However, Riemer et al. conclude that since 316 L exhibits high ductility (53.7% elongation to failure), even in the as-built

Sepehr Hatami, Taoran Ma, and Ola Lyckfeldt, RISE IVF AB, Argongatan 30, 431 53 Mölndal, Sweden; Taina Vuoristo, Swerim AB, Isafjordsgatan 28A, 164 40 Kista, Sweden; and Jens Bertilsson, Sigma Industry East North AB, Rådhusesplanaden 2C, 903 28 Umeå, Sweden. Contact e-mails: Sepehr.hatami@ri.se, Taoran.ma@ri.se, taina.vuoristo@swerim.se, jens.bertilsson@sigma.se, and ola.lyckfeldt@ri.se.

condition, the material does not suffer severely from SLM process-induced defects such as pores and residual stress (Ref 10).

The objective of this research is to understand the effect of layer thickness and postmachining operation on fatigue strength. Regarding layer thickness, specimens are produced with 30 and 50 μm layer thickness. The specimens are then fatigue tested in two conditions, (1) as-printed and (2) postmachined. The specimens are characterized with respect to parameters that are known to affect the fatigue strength of materials such as surface roughness, residual stress, and microstructure.

2. Materials and Methods

2.1 Powder Properties

The material used in this investigation was a gas-atomized 316 L stainless steel powder manufactured by Höganäs AB (Höganäs, Sweden). The chemical composition of the powder is given in Table 1. According to the material specification provided by the powder manufacturer, the powder exhibited an apparent density of 4.09 g/cm^3 and a flowrate (Hall) of 16 s/50 g. The specific surface area of the powder was determined by gas adsorption analysis based on the BET principle. BET surface area equal to 0.030 m^2/g was measured using a Gemini VII apparatus from Micrometrics (Norcross, Georgia, USA).

Powder particle size was measured by laser diffraction using a Mastersizer 3000 equipment from Malvern (Malvern, UK). Particle size measurements were repeated four times, and the equivalent diameter for D10, D50, and D90 was averaged, see Table 2. D10, D50, and D90 values correspond to the particle sizes at the 10, 50, and 90 percent points on the cumulative particle size distribution.

2.2 Specimen Manufacturing

All fatigue specimens were manufactured using a SLM 125 HL system from SLM Solutions GmbH (Lübeck, Germany). This machine has a build envelope of 125 × 125 × 125 mm^3 (reduced by substrate plate thickness) and a single 400-W fiber laser. The SLM process parameters used in this investigation were provided by SLM Solutions GmbH and were specifically developed for 316 L stainless steel. Fatigue specimens were manufactured by lowering increments of the build plate by 30 and 50 μm (henceforth referred to as layer thickness). Parameter setting designations 316L_SLM_MBP3.0_30_CE1_400W_Stripes_V1.1 and 316L_SLM_MBP3.0_50_CE1_400W_Stripes_V1.1 were used for 30 and 50 μm layer thickness, respectively. The specimens were manufactured without the use of support structures and were built directly on the build plate. The build direction is parallel to the longitudinal axis of the specimens.

All test specimens were manufactured with a laser spot size of 65 μm using a stripe pattern. In these SLM runs, first the contour and then the core of the surface are shaped. The contour consists of two borders, and one fill contour.

Following the recommendations from SLM Solutions GmbH, the powder was dried at 60°C (for a minimum 24 h) and then sieved prior to being loaded into the SLM machine. The sieving operation was performed using a PSM 100 unit (manufactured by SLM Solutions GmbH) with a 75-μm mesh

Table 1 Chemical composition (in wt.%) of 316L gas-atomized powder as stated in the material specification

Fe	C	Mo	Ni	Mn	Cr	Si	O
Bal.	0.015	2.5	12.7	1.5	16.9	0.7	0.059

Table 2 Particle size of the investigated 316 L stainless steel powder measured by laser diffraction

Particle size	D10	D50	D90
Average	30.9	45.4	65.9
SD	0.6	0.4	0.5
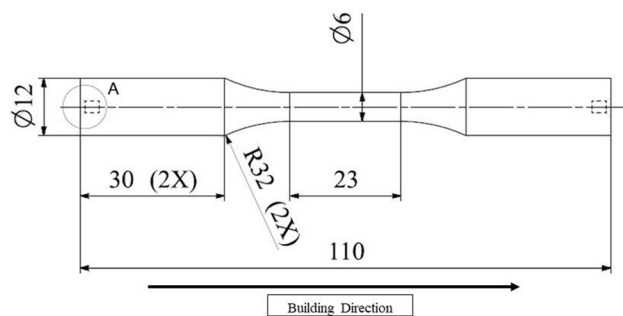
Fig. 1 Specimen geometry for high cycle fatigue tests

in an argon atmosphere. In order to prevent excessive oxidation during SLM processing, argon 4.8 premium gas from AGA GAS AB (Lidingö, Sweden) was used. The building platform was kept at 200°C during the entire process to limit distortion. The produced specimens were removed from the build plate using wire electrical discharge machining and were not stress relieved.

Fatigue specimens for the as-printed and postmachined batch of specimens were manufactured with 1 mm of machining allowance on the grip heads. This was done in order to minimize misalignment when mounting the specimens in the testing equipment. The postmachined batch of fatigue specimens was manufactured with 3 mm of machining allowance in the gage section of the specimen. The machining procedure was turning by lathe followed by manual polishing in the longitudinal direction of the specimen in order to remove any machining marks or scratches on the surface. The final dimension and geometry of the fatigue specimens are shown in Fig. 1. This geometry complies with ISO 1099.

2.3 Surface Roughness

Surface roughness was measured with a Sensofar S neox instrument (Terrassa, Spain) using confocal fusion. Confocal fusion is a technique that combines confocal microscopy with focus variation. Measurements were taken with a 20 × magnification objective, and the images were stitched to cover an area of 2.2 mm × 1.6 mm. The lateral resolution of the

Table 3   Surface roughness values (and the standard deviations) of as-printed and postmachined specimens

Layer thickness, μm	As printed			Postmachined		
	Sa, μm	Sq, μm	S10z, μm	Sa, μm	Sq, μm	S10z, μm
30	13.1 ± 0.8	15.9 ± 1.0	69.4 ± 11.7	0.5	0.7	5.0 ± 1.1
50	15 ± 2.0	18.5 ± 2.5	71.8 ± 5.3	0.5	0.7 ± 0.1	4.0 ± 0.4
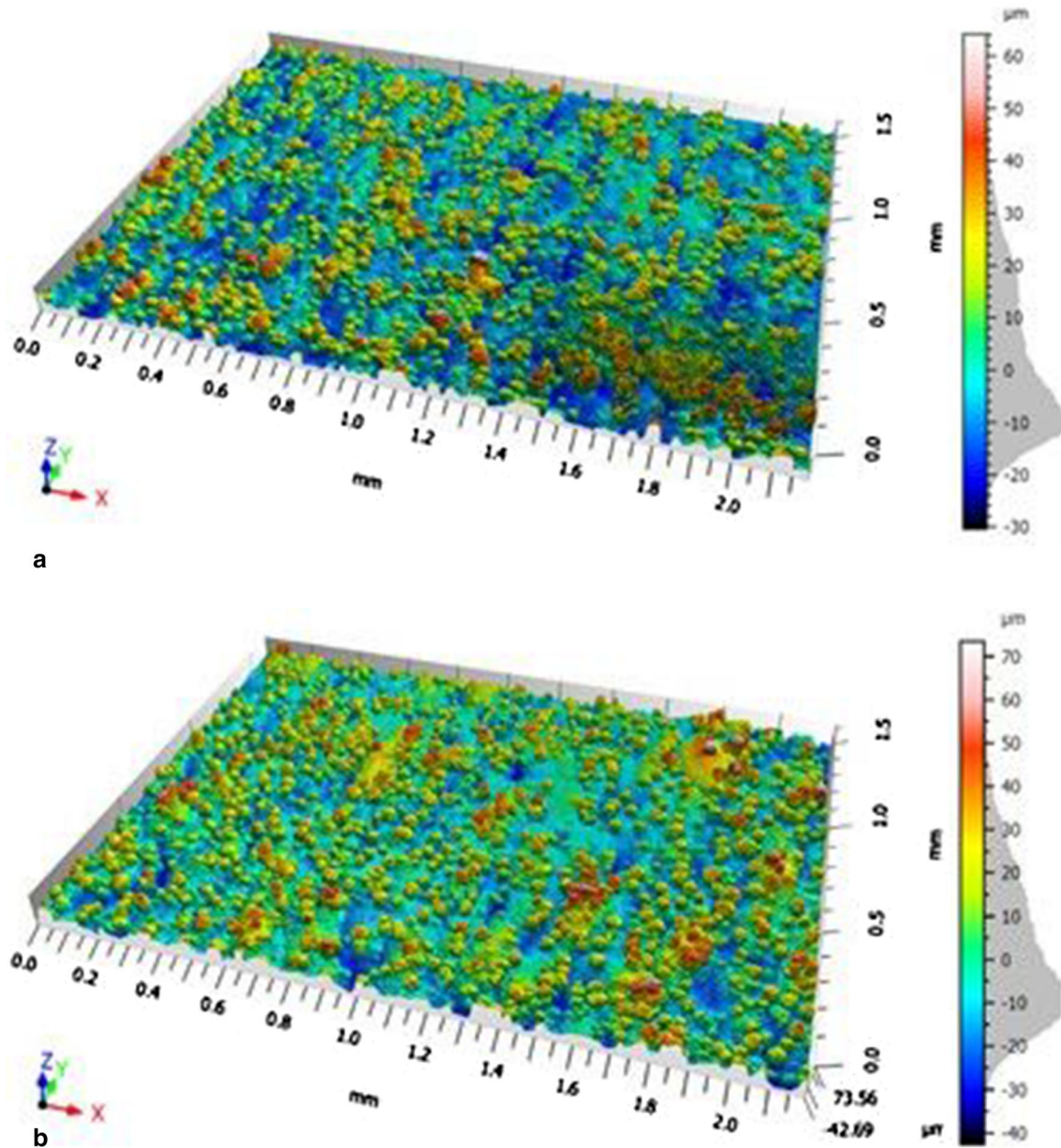
Fig. 2   3D view of as-printed surfaces manufactured with a) 30 μm and b) 50 μm layer thickness

measurements was 0.645 μm. In all the measurements, the short wavelength noise was removed with a spatial median denoise filter with a window size of 5 × 5 points. Form removal was carried out using 3rd degree polynomial, and the non-measured points were filled in. The non-measured point ratio is typically below 2% and does not exceed 4%. Surfaces were characterized according to ISO 25178-2, using Sa (i.e., arithmetic mean height), Sq (i.e., root-mean-square height), and S10z (ten-point height pruning = 5%). Measurements were taken on the gage length of the specimens on five random locations. The mean value of the measurements was used to compare the surfaces.
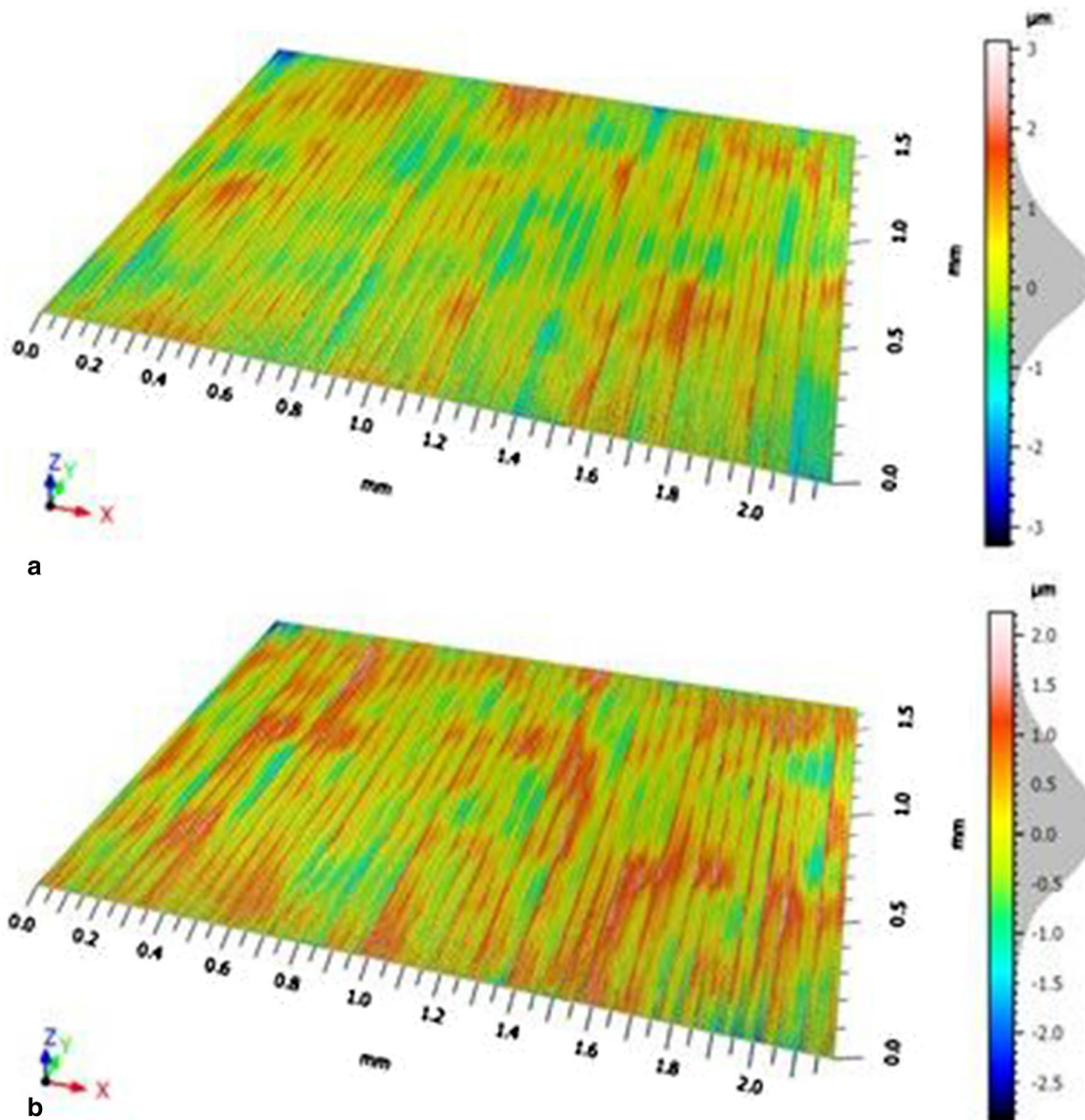
Fig. 3 3D view of postmachined surfaces manufactured with a) 30 μm and b) 50 μm layer thickness
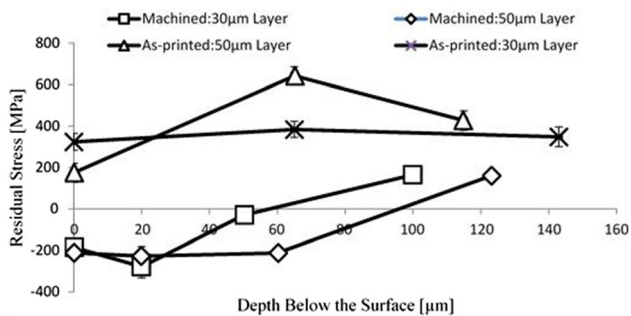

**Fig. 4** Residual stress profiles measured along the longitudinal axis of fatigue specimens

2.4 Residual Stress

Residual stress measurements were taken by x-ray diffraction (XRD) using a XStress 3000G2R equipment from Stresstech Oy (Vaajakoski, Finland). All measurements were taken in an accredited laboratory in accordance with the SS-EN 15304:2008 standard (Ref 11). The diffractometer was equipped with a chromium x-ray tube ($\lambda = 0.210314$ nm) with a 30 kV and 6.6 mA power supply. Measurements were taken with a 1-mm collimator. The lattice plane (311) with a 2θ diffraction peak located at 152.3° was measured. The modified $\sin^2\Psi$ method was used with 5 psi angles ($\pm 40°$, $\pm 33.8°$, $\pm 27°$, $\pm 18.7°$, $0°$). Residual stresses were calculated based on Hooke's law and elastic strain theory, using Young's modulus of 196 GPa and a Poisson's ratio of 0.28. The measurement data were analyzed using Xtronic 1.12.1 software, and cross-correlation was used for peak fitting. Residual stress profiles were created by measuring the stress at different depths below the surface of the specimen. For these measurements, a specific amount of material was removed from the surface by means of electropolishing (Struers Movipol) with A2 electrolyte from Struers (Ballerup, Denmark) and following their recommended settings. It should be noted that the high surface roughness of as-printed samples can lead to an inhomogeneous electropolishing effect. To circumvent this issue and ensure a uniform material removal, as-printed
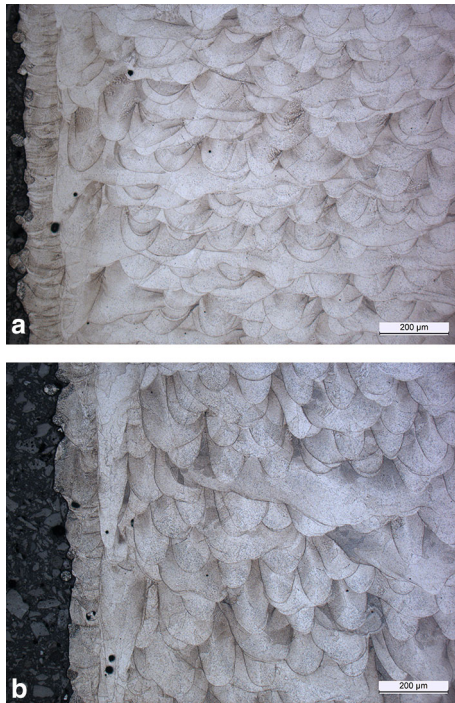
Fig. 5 As-printed microstructure of 316L stainless steel parallel to the build direction: a) 30 μm layer thickness and b) 50 μm layer thickness. Micrographs courtesy of Höganäs AB, Sweden
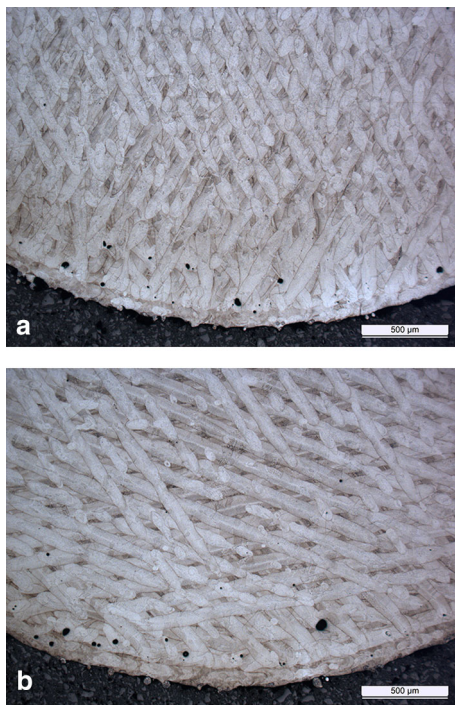
Fig. 6 As-printed microstructure of 316L stainless steel perpendicular to the build direction: a) 30 μm layer thickness and b) 50 μm layer thickness. Micrographs courtesy of Höganäs AB, Sweden

surfaces were gently grinded by hand using sandpaper with 200 grit size prior to electropolishing.

2.5 High Cycle Fatigue

All fatigue tests were performed at room temperature with a sinusoidal force function and frequency of 20 Hz. The failure criterion was the complete separation of the specimen. The tests were carried out at a stress ratio of $R = 0.1$, and 2×10^6 cycles were considered as run-out. A minimum of 14 samples for each batch of specimens was tested at four stress amplitudes: 247.5, 202.5, 157.5, and 112.5 MPa. The only exception was the batch of postmachined specimens manufactured with 30 μm layer thickness. For this batch, due to an inadequate number of specimens, only eight samples were tested. The tests were carried out in a servo-hydraulic material testing machine from MTS (Eden Prairie, Minnesota, USA). The machine was equipped with a 100-kN load cell and hydraulic collet grips. The fatigue tests were controlled by force using a FlexTest GT controller and MTS MultiPurpose TestWare software. Machine alignment was performed according to ISO 23788:2012 (Ref 12).

2.6 Microstructure

Microstructure evaluations were carried out on cross sections parallel and perpendicular to the build direction. The metallographic samples were extracted away from the fracture surface but within the gage length of the specimen. Microstructure examinations were performed using optical microscopy, and samples were etched using a solution consisting of 45 ml distilled water + 30 ml HCL +15 ml HNO_3. Fracture surfaces were examined by means of stereo and scanning electron microscopy (SEM) with a secondary electron detector.

2.7 Hardness and Porosity

Vickers hardness testing was performed on the as-printed specimens on cross sections parallel to the build direction. The hardness of the core of the specimens was determined based on the average of five indentations with an applied load of 1 kg (i.e., HV1). The surface hardness was measured with micro-indentations with an applied load of 50 grams (i.e., HV0.05). Approximately thirty indents were made on the border of the specimens, and the average hardness was calculated. Porosity measurements were taken on cross sections perpendicular to the build direction on an area including both the core and the border. The samples were investigated with light optical microscopy, and the porosity was measured with 12.5× magnification using an image analysis software.

3. Results and Discussion

3.1 Surface Roughness

As shown in Table 3, as-printed specimens are significantly rougher than postmachined samples. Furthermore, in the as-printed condition, surface roughness seems to be slightly lower for samples manufactured with 30 μm layer thickness as compared to those manufactured with 50 μm layer thickness, see Table 3.

It is worth noting that in the as-printed condition, while the difference in roughness was only a few microns, the production time was significantly lower for specimens manufactured with 50 μm layer thickness as compared to those manufactured with

Table 4 Porosity measurements by image analysis

Layer thickness	Condition	Porosity, area%	Total Amount of Pores
30	As printed	0.1	97
30	Postmachined	0.03	30
50	As printed	0.27	270
50	Postmachined	0.23	207
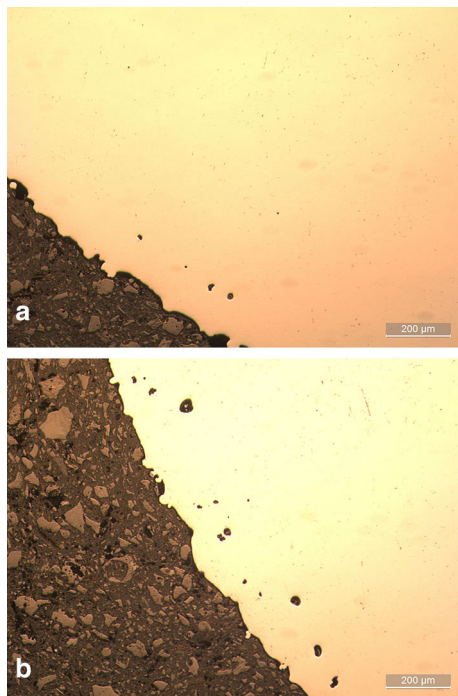
Fig. 7 Near-surface porosity in polished as-printed specimens perpendicular to the build direction: a) 30 μm layer thickness and b) 50 μm layer thickness

30 μm layers. The production time decreased by 58% when increasing the layer thickness from 30 to 50 μm.

The overall surface topography of the as-printed and postmachined specimens is shown in Fig. 2 and 3, respectively. Histogram of the height distribution is presented next to the scale bar in Fig. 2 and 3. The distribution is slightly narrower for as-printed specimens manufactured with 30 μm layer thickness as compared to their 50-μm counterparts. After the machining operation, the distribution becomes considerably narrower and ranges from approximately -1 μm to $+2$ μm, see Fig. 3. The height distribution in the as-printed condition is significantly wider than in the postmachined condition.

The high surface roughness of as-printed specimens has a clear negative impact on the fatigue strength. Unmelted powder particles at the surface will act as stress raisers and thereby lower the fatigue performance (Ref 1, 13). The postmachining process removes the unmelted particles which are potential crack initiation sites (Ref 1). Uhlmann et al. observed a lower fatigue life in as-printed 316 L stainless steel as compared to postmachined specimens and attributed this discrepancy to surface roughness (Ref 7).

3.2 Residual Stress

Residual stress was measured along the longitudinal axis of the samples parallel to the build direction. As can be seen in Fig. 4, as-printed samples possess high tensile residual stress at the surface and up to ~ 120–140 μm below the surface. In contrast, postmachined specimens exhibit compressive residual stress at the surface and up to ~ 50 μm and ~ 90 μm below the surface. The machining process induces compressive stresses in the feed direction (Ref 14), which is along the longitudinal axis of the specimens. It is a well-known fact that compressive surface residual stresses are beneficial for fatigue. In addition, the postmachining operation removes the surface portion of the material which is under tensile stress.

3.3 Microstructure

The microstructure was evaluated in both directions. Figure 5 and 6 show the microstructure parallel and perpendicular to the build direction, respectively. The microstructure of the border of the specimen is different from that of the core, see Fig. 5 and 6. The observed difference is due to the SLM process parameters which are used for shaping borders, fill contour, and the core of each layer. It is worth noting that the border and fill contour parameters have a significant impact on the surface integrity of the as-printed specimens. The melt pools seem to be slightly shallower in specimens manufactured with 30 μm layer thickness (Fig. 5a) as compared to those built with 50 μm layers (Fig. 5b). The path of the laser stripe can be clearly seen in Fig. 6. In addition, near-surface porosity is prevalently found close to the border of the samples, see Fig. 6.

3.4 Hardness and Porosity

For as-printed specimens manufactured with 30 and 50 μm layer thickness, the average core hardness was 226 ± 6 and 233 ± 6 (HV1), respectively. The average surface hardness of as-printed specimens manufactured with 30 and 50 μm was 279 ± 21 and 253 ± 19 (HV0.05), respectively. Difference in surface hardness is most likely related to SLM process parameters.. The process parameters used for specimens manufactured with 30 μm layer thickness may result in a finer surface microstructure and grain size. The finer microstructure is expected to have a positive impact on fatigue strength (Ref 15).

The result of the porosity measurements is shown in Table 4. It is worth mentioning that by image analysis it is not possible to differentiate between porosity and other forms of defects such as oxides and carbides.

In general, as-printed samples possess a higher porosity content as compared to the postmachined variant. This is mainly due to the presence of pores close to the surface which are removed by the postmachining operation, see Fig. 7.
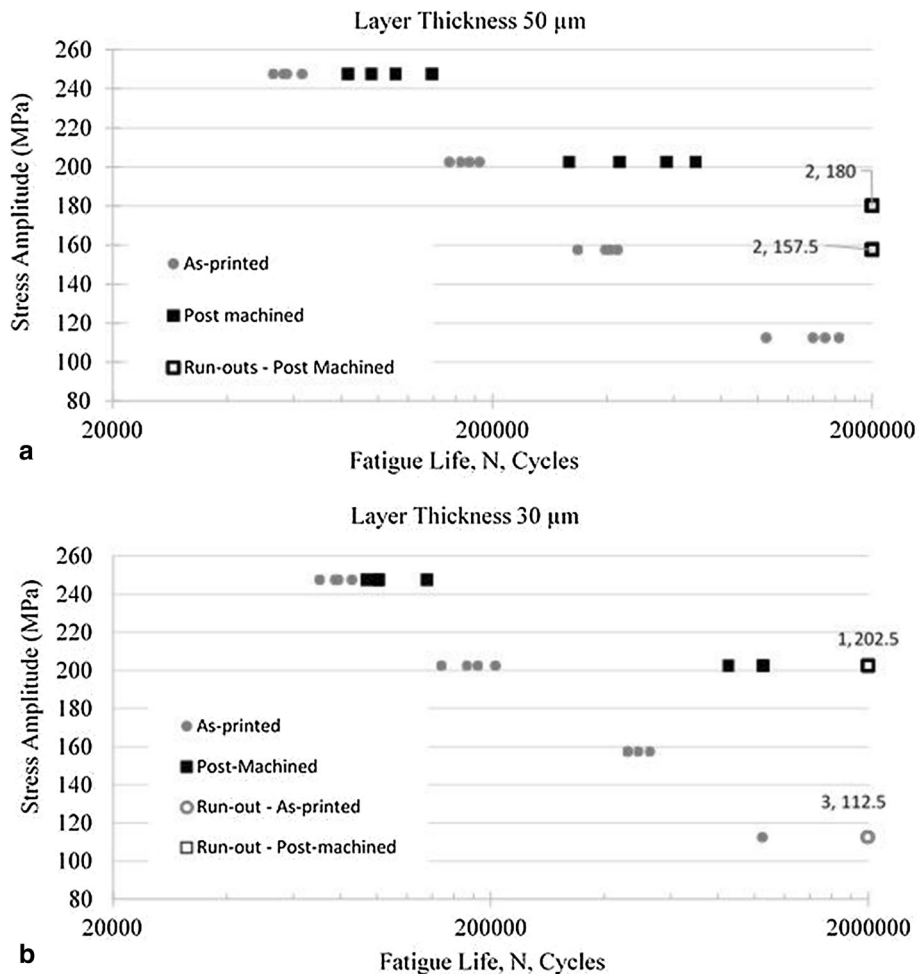
Fig. 8 Fatigue data for 316L stainless steel manufactured with a) 50 μm and b) 30 μm layer thickness. Data labels show the number of run-outs and the stress amplitude

Furthermore, a considerably higher content of porosity is found in samples manufactured with 50 μm layer thickness as compared to those manufactured with 30 μm. This is most likely due to insufficient energy input which can lead to inadequate melting and lack of fusion. Higher porosity content, especially close to the surface, increases the risk of crack initiation under fatigue.

3.5 Fatigue Tests

Fatigue data from specimens manufactured with 50 and 30 μm layer thickness are illustrated in Fig. 8. The data show that regardless of the layer thickness, machined samples exhibit a higher fatigue strength as compared to as-printed specimens.

At 5×10^5 cycles the fatigue strength of postmachined specimens is more than 50 MPa higher than that of as-printed specimens. These results agree with the surface roughness, residual stress, porosity, and hardness measurements. Postmachined samples have a much lower surface roughness as compared to the as-printed specimens (see Table 3), and they benefit from surface compressive residual stresses (see Fig. 4) and a lower content of surface porosity (see Table 4). These are the main reasons for reaching a higher fatigue strength after machining (Ref 16).

Figure 9 illustrates the impact of layer thickness on the fatigue strength of as-printed and postmachined specimens,

respectively. The data show that regardless of the condition of the specimens (i.e., as printed or postmachined) the difference in fatigue strength between specimens manufactured with 30 and 50 μm appears to be small.

Figure 9 shows fatigue data for 316 L stainless steel in a) as-printed and b) postmachined conditions manufactured with 30 and 50 μm layer thickness. Data labels show the number of run-outs and the stress amplitude.

Although further interpretation of the results is not statistically secured, the data in Fig. 9(a) suggest a slightly higher fatigue strength for as-printed specimens fabricated with 30 μm layer thickness as compared to those manufactured with 50 μm layer thickness. A similar trend can be deduced from Fig. 9(b) for postmachined specimens. However, as described under heading 2.5, the postmachined batch of specimens manufactured with 30-μm layers consisted of only eight specimens which were tested at two load levels. Hence, further testing is needed in order to draw conclusions. Nonetheless, the porosity measurements shown in Table 4 indicate a significantly lower pore content in specimens manufactured with 30-μm layers as compared to those fabricated with 50 μm. This observation favors a higher fatigue strength for samples manufactured with 30 μm as compared to those manufactured with 50 μm. Comparison of the data in Fig. 9(a) and (b) suggests a greater scatter in fatigue data in the postmachined condition than in the
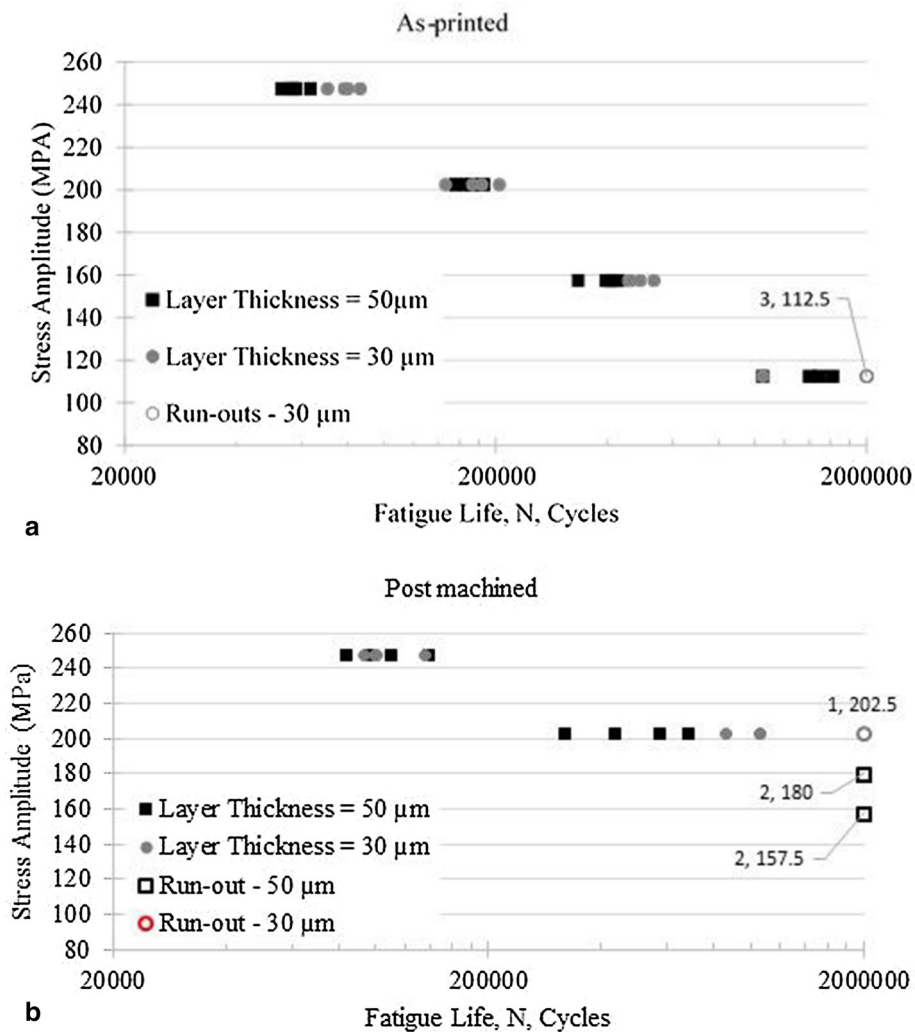
Fig. 9 Fatigue data for 316L stainless steel in a) as-printed and b) postmachined conditions manufactured with 30 and 50 μm layer thickness. Data labels show the number of run-outs and the stress amplitude

as-printed condition. This could be a consequence of the machining operation with which the main causes of crack initiation, namely, surface porosity and high surface roughness, are eliminated. Hence, fatigue is initiated from the more randomly distributed defects in the core of the specimens.

All the fatigue data presented thus far are plotted in Fig. 10. In addition, Fig. 10 illustrates data on conventionally produced 316 LN stainless steel tested at the same stress ratio but a lower frequency (i.e., 10 Hz) (Ref 17). The plot shows that while the fatigue strength of conventionally produced 316 LN is slightly higher than as-printed 316 L material, it is significantly lower than SLM-produced 316 L after machining. Elangeswaran et al. also report a higher fatigue strength for SLM produced and postmachined 316 L specimens as compared to conventionally manufactured 316 L material (Ref 1). From Fig. 10 it is clear that the positive impact of the postmachining operation is larger than that of lowering the layer thickness from 50 to 30 μm.

3.6 Fractography

The fracture surface of the specimens that were tested at a high stress amplitude (e.g., 247 MPa) is predominantly very rough in appearance and exhibits large areas of severe plastic

deformation indicating the final stage of the fatigue process, namely, ultimate ductile failure, see Fig. 11(a). On the other hand, specimens that were tested at lower stress amplitudes (e.g., 112 MPa) exhibit fracture surfaces which are mainly flat, an indication of a more incremental crack propagation. This pattern can be seen in Fig. 11(b).

Fracture surfaces were also examined by means of scanning electron microscopy (SEM) combined with a secondary electron detector. Figure 12(a) shows potential crack initiation sites.

As can be seen, spherical pores are found close to the surface of the specimen. Frequently, the internal surface of these pores contains concentric ridges, see Fig. 12(b). This type of defect has been reported by Qiu et al. in Ti-6Al-4 V material. The pores seen in Fig. 12(b) are different to those formed due to lack of fusion or gas entrapment (Ref 18). Lack of fusion defects is typically irregular in shape, and pores created by gas entrapment do not contain ridges. According to Qui et al., pores with ridges are most likely formed during laser scanning and are created due to incomplete re-melting of a localized surface of a previous layer (Ref 18). They speculate that this incompletely re-melted point will slow down the spreading of the molten material in its proximity and will result in a volume
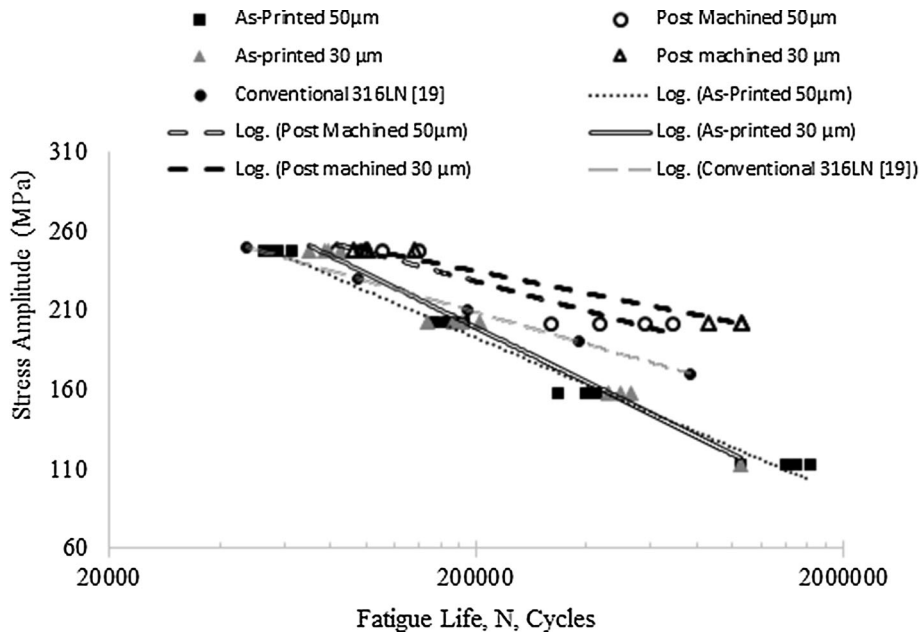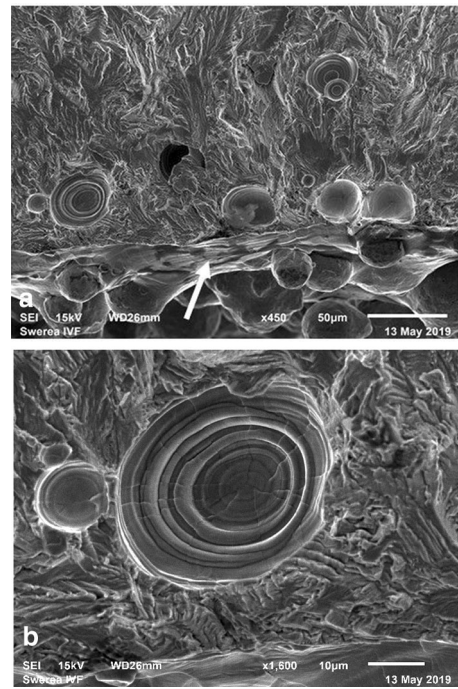
Fig. 10 Influence of layer thickness and postmachining operation on the fatigue strength of SLM-manufactured 316L stainless steel. Run-outs are excluded from the plot and the curve fitting
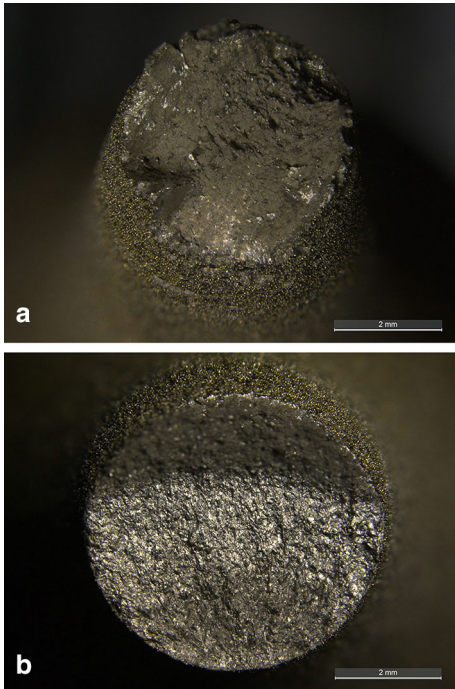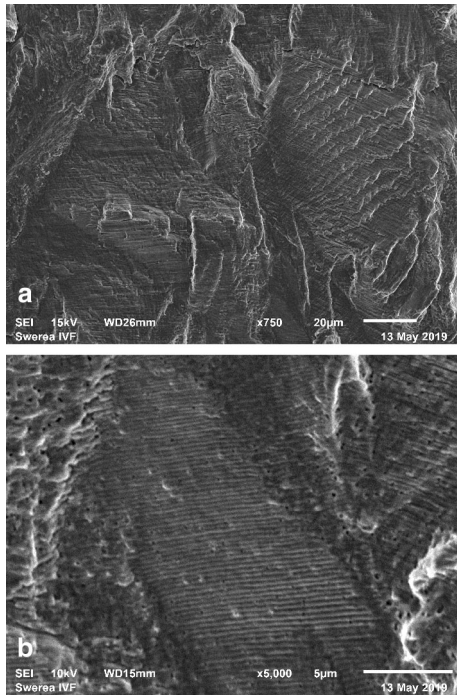

Fig. 11 Fracture surface of specimens manufactured with 50 μm layer thickness and tested in the as-printed condition: a) stress amplitude = 247 MPa, cycle to failure = 57,561. b) Stress amplitude = 112 MPa, cycle to failure = 1,501,941

Fig. 12 Fracture surface of an as-printed 316L stainless steel specimen manufactured using 50 μm layer thickness: a) possible crack initiation sites near the surface, arrow indicating surface of the specimen, and b) pores with ridges inside

where molten metal is unable to penetrate. Qui et al. state that the ridges seem to represent the progress of solidification fronts where there is no feeding of the molten metal (Ref 18). However, Saiz et al. have observed the ridging phenomenon in wetting experiments with liquid metals on sapphire substrate. They claim that ridges are formed at a triple line (i.e., contact between gas, solid and liquid) in response to the vertical
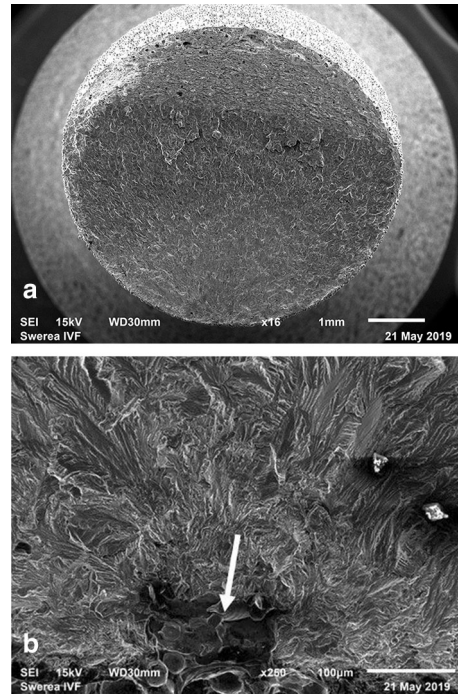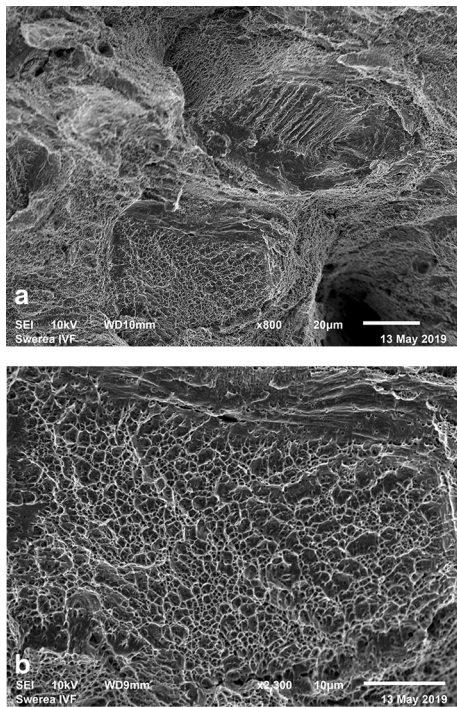
component of force from surface tension (Ref 19, 20). Local atomic diffusion takes place at high temperatures, and the substrate can deform at the triple point, resulting in a ridge (Ref 19). The temperatures reached during SLM processing are sufficiently high to assist atomic diffusion, and deformation of the material can take place with relative ease. The ridge formed can hinder the melt from spreading. However, in certain

Fig. 13 Crack propagation due to fatigue in 316L stainless steel tested in the as-printed condition: a) transgranular fracture and b) fatigue striation
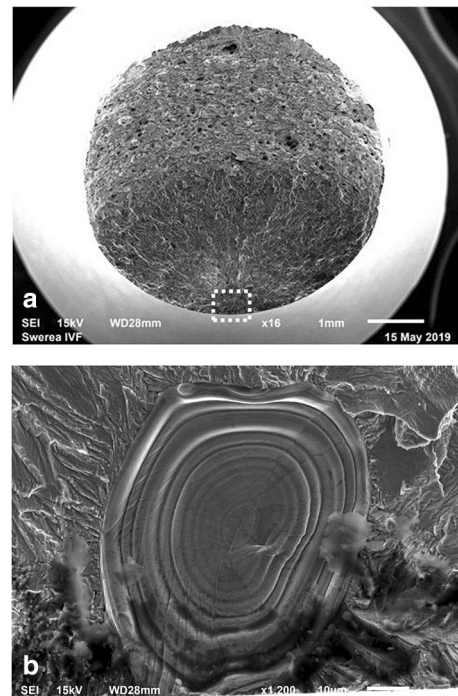

Fig. 14 Fracture surface of 316L stainless steel fatigue tested in the as-printed condition: a) ultimate ductile failure and b) dimpled rupture

Fig. 15 Fracture surface of an as-printed 316L stainless steel specimen manufactured using 30 μm layer thickness: a) overall fracture surface and b) crack initiation site close to the surface indicated by the arrow

Fig. 16 Fracture surface of a postmachined specimen manufactured with 50 μm layer thickness: a) macroscopic view of the entire fracture and b) higher magnification of the initiation site, as shown by the boxed region in image a. Black marks in the image are contamination

conditions the melt can break away from the ridge and start a new ridge by the same mechanism (Ref 19). It is worth noting that ridges were found on specimens prior to testing; hence, their formation cannot be a consequence of fatigue testing.

Thus, it seems reasonable to assume that pores containing ridges are a direct consequence of the SLM process.

The main portion of the fracture surface exhibits a transgranular mode of fracture, see Fig. 13(a). Striation marks indicative of the cyclic crack propagation are found on the fracture surface, see Fig. 13(b). The final stage of fatigue failure occurs in a ductile manner, and the dimpled microstructure is a clear sign of this fracture mode, see Fig. 14.

The fracture surface of as-printed specimens manufactured with 30 μm layer thickness is in general similar to those manufactured with 50 μm layer thickness. Crack initiation sites are found close to the surface, and defects initiating the cracks are mainly process related, Fig. 15. As can be seen in Fig. 15(b), the initiation site (in this specific specimen) is most likely caused by a lack of fusion void.

A macroscopic image of the fracture surface of a postmachined specimen is shown in Fig. 16(a). Although the machining operation removes the pores and voids near the surface of the specimen, fatigue cracks seem to initiate from pores similar to those shown in Fig. 12(b).

4. Conclusions

In this study, high cycle fatigue tests were performed on SLM-produced specimens in as-printed and postmachined conditions. The influence of layer thickness and postmachining on the fatigue strength of SLM-manufactured 316 L stainless steel was evaluated. The following conclusions can be drawn from this investigation:

- Increasing the layer thickness from 30 to 50 μm has a minor negative impact on fatigue strength; however, it has a major positive impact on the productivity of the SLM process. In both as-printed and postmachined conditions, the data suggest a slight increase in fatigue strength when using 30-μm layers.
- A significantly higher content of pores is found in samples manufactured with 50 μm layer thickness than in those fabricated with 30 μm.
- The impact of the postmachining operation on fatigue is far greater than that of the layer thickness.
- In the as-printed condition, fatigue strength suffers from high surface roughness, tensile surface residual stresses, and defects such as pores and lack of fusion.
- Improvement of fatigue strength after machining is due to lower surface roughness, the presence of compressive surface residual stresses, and removal of surface porosity.
- The fatigue strength of SLM-manufactured 316 L stainless steel in the as-printed condition seems to be slightly lower than that of conventionally produced 316 LN stainless steel material. However, after machining, the fatigue strength of SLM-produced parts is considerably higher than that of their conventionally produced counterparts.

References

1. C. Elangeswaran, A. Cutolo, G.K. Muralidharan, C. de Formanoir, F. Berto, K. Vanmeensel, and B. Van Hooreweder, Effect of Post-Treatments on the Fatigue Behaviour of 316L Stainless Steel Manufactured by Laser Powder Bed Fusion, *Int. J. Fatigue*, 2019, **123**, p 31–39. https://doi.org/10.1016/j.ijfatigue.2019.01.013
2. R. Shrestha, J. Simsiriwong, N. Shamsaei, M.S. Thompson, and L. Bian, "Effect of Build Orientation on the Fatigue Behavior of Stainless Steel 316L Manufactured via a Laser Powder Bed Fusion Process," *27th Annual International Solid Freeform Fabrication Symposium*, 2016, p 605–616. https://pdfs.semanticscholar.org/e8b3/b9988d312d59816ac07a0e21881413efdf11.pdf. Accessed 27 May 2020
3. T. Wohlers, I. Campbell, O. Diegel, R. Huff, and J. Kowen, Cost Benefits of DfAM, *Wohlers Report*, Wohlers Associates Inc., 2019, p 221–225
4. S. Afkhami, M. Dabiri, S.H. Alavi, T. Björk, and A. Salminen, Fatigue Characteristics of Steels Manufactured by Selective Laser Melting, *Int. J. Fatigue*, 2019, **122**, p 72–83. https://doi.org/10.1016/j.ijfatigue.2018.12.029
5. G.E. Dieter, *Mechanical Metallurgy*, 3rd ed., McGraw-Hill, Boston, 1986
6. T.M. Mower and M.J. Long, Mechanical Behavior of Additive Manufactured, Powder-Bed Laser-Fused Materials, *Mater. Sci. Eng., A*, 2016, **651**, p 198–213. https://doi.org/10.1016/j.msea.2015.10.068
7. E. Uhlmann, C. Fleck, G. Gerlitzky, and F. Faltin, Dynamical Fatigue Behavior of Additive Manufactured Products For a Fundamental Life Cycle Approach, *Procedia CIRP*, 2017, **61**, p 588–593. https://doi.org/10.1016/j.procir.2016.11.138
8. B. Blinn, M. Klein, C. Gläßner, M. Smaga, J. Aurich, and T. Beck, An Investigation of the Microstructure and Fatigue Behavior of Additively Manufactured AISI, 316L Stainless Steel with Regard to the Influence of Heat Treatment, *Metals (Basel)*, 2018, **8**(4), p 220. https://doi.org/10.3390/met8040220
9. M. Zhang, C.-N. Sun, X. Zhang, J. Wei, D. Hardacre, and H. Li, Predictive Models for Fatigue Property of Laser Powder Bed Fusion Stainless Steel 316L, *Mater. Des.*, 2018, **145**, p 42–54. https://doi.org/10.1016/j.matdes.2018.02.054
10. A. Riemer, S. Leuders, M. Thöne, H.A. Richard, T. Tröster, and T. Niendorf, On the Fatigue Crack Growth Behavior in 316L Stainless Steel Manufactured by Selective Laser Melting, *Eng. Fract. Mech.*, 2014, **120**, p 15–25. https://doi.org/10.1016/j.engfracmech.2014.03.008
11. Non-Destructive Testing - Test Method for Residual Stress Analysis by X-Ray Diffraction, *Swedish Stand. Inst.*, 2008, **SS-EN 1530**
12. Metallic Materials—Verification of the Alignment of Fatigue Testing Machines, *Int. Organ. Stand.*, 2012, **ISO 23788:**

13. K. Solberg and F. Berto, What Is Going on with Fatigue of Additively Manufactured Metals?, *Mater. Des. Process. Commun.*, 2019. https://doi.org/10.1002/mdp2.84

14. D.Y. Jang, T.R. Watkins, K.J. Kozaczek, C.R. Hubbard, and O.B. Cavin, Surface Residual Stresses in Machined Austenitic Stainless Steel, *Wear*, 1996, **194**(1–2), p 168–173. https://doi.org/10.1016/0043-1648(95)06838-4

15. A. Di Schino, M. Barteri, and J.M. Kenny, Effects of Grain Size on the Properties of a Low Nickel Austenitic Stainless Steel, *J. Mater. Sci.*, 2003, **38**(23), p 4725–4733. https://doi.org/10.1023/A:1027470917858

16. E. Uhlmann, G. Gerlitzky, and C. Fleck, Fatigue Behavior of Additive Manufactured Parts in Different Process Chains - An Experimental Study, *Ann. Int. Solid Freefrom Fabricat. Sympo.*, 2017, **2**, p 48–60

17. J.P. Strizak, H. Tian, P.K. Liaw, and L.K. Mansur, Fatigue Properties of Type 316LN Stainless Steel in Air and Mercury, *J. Nucl. Mater.*, 2005, **343**(1–3), p 134–144. https://doi.org/10.1016/j.jnucmat.2005.03.019

18. C. Qiu, N.J.E. Adkins, and M.M. Attallah, Microstructure and Tensile Properties of Selectively Laser-Melted and of HIPed Laser-Melted Ti-6Al-4V, *Mater. Sci. Eng., A*, 2013, **578**, p 230–239. https://doi.org/10.1016/j.msea.2013.04.099

19. E. Saiz, A.P. Tomsia, and R.M. Cannon, Ridging Effects on Wetting and Spreading of Liquids on Solids, *Acta Mater.*, 1998, **46**(7), p 2349–2361. https://doi.org/10.1016/S1359-6454(98)80016-5

20. I. Yadroitsev, *Selective Laser Melting*, Lambert Academic Publishing, Saarbrucken, 2009

Publisher's Note Springer Nature remains neutral with regard to jurisdictional claims in published maps and institutional affiliations.